Development/Plasticity/Repair

$p19^{Ink4d}$ and $p21^{Cip1}$ Collaborate to Maintain the Postmitotic State of Auditory Hair Cells, Their Codeletion Leading to DNA Damage and p53-Mediated Apoptosis

Heidi Laine,[1] Angelika Doetzlhofer,[3] Johanna Mantela,[1] Jukka Ylikoski,[1] Marikki Laiho,[2] Martine F. Roussel,[4] Neil Segil,[3] and Ulla Pirvola[1]

[1]Institute of Biotechnology and [2]Molecular Cancer Biology Program, Biomedicum Helsinki, University of Helsinki, 00014 Helsinki, Finland, [3]Gonda Department of Cell and Molecular Biology, House Ear Institute, Los Angeles, California 90057, and [4]Department of Tumor Biology and Genetics, St. Jude Children's Research Hospital, Memphis, Tennessee 38105

Sensory hair cells of the auditory organ are generated during embryogenesis and remain postmitotic throughout life. Previous work has shown that inactivation of the cyclin-dependent kinase inhibitor (CKI) $p19^{Ink4d}$ leads to progressive hearing loss attributable to inappropriate DNA replication and subsequent apoptosis of hair cells. Here we show the synergistic action of another CKI, $p21^{Cip1}$, on cell cycle reactivation. The codeletion of $p19^{Ink4d}$ and $p21^{Cip1}$ triggered profuse S-phase entry of auditory hair cells during a restricted period in early postnatal life, leading to the transient appearance of supernumerary hair cells. In addition, we show that aberrant cell cycle reentry leads to activation of a DNA damage response pathway in these cells, followed by p53-mediated apoptosis. The majority of hair cells were absent in adult cochleas. These data, together with the demonstration of changing expression patterns of multiple *CKIs* in auditory hair cells during the stages of early postnatal maturation, show that the maintenance of the postmitotic state is an active, tissue-specific process, cooperatively regulated by several CKIs, and is critical for the lifelong survival of these sensory cells.

Key words: **cyclin-dependent kinase inhibitor; proliferation; DNA damage; apoptosis; development; inner ear**

Introduction

The inner ear houses the auditory and vestibular sensory epithelia, which are required for hearing and balance function, respectively. Hair cells (HCs) within these sensory epithelia function as mechanotransducers, converting a mechanical stimulus into an electrical signal. In mice, progenitors of the organ of Corti, the auditory sensory epithelium, make their final cell division between embryonic day 12.5 (E12.5) and E14.5 (Ruben, 1967). These terminal mitoses are followed by the onset of differentiation into the mosaic of HCs and supporting cells that characterizes the mature organ of Corti. Both HCs and supporting cells subsequently maintain the postmitotic state throughout the life of the animal. Thus, neither HCs nor supporting cells of the organ of Corti divide under normal conditions or in response to damage. This lack of regenerative ability means that HC loss leads to permanent deafness (for review, see Matsui et al., 2005).

Maintenance of the postmitotic state of HCs has been shown previously to require the cyclin-dependent kinase inhibitor (CKI) $p19^{Ink4d}$ (Chen et al., 2003). Cyclin-dependent kinase inhibitors function by binding to and inhibiting the activity of cyclin-dependent kinases (CDKs), which, along with their positively acting cofactors, the cyclins, are part of a family of kinases that function in both promoting normal cell cycle progression and surveillance and checkpoint functions in the cell cycle (for review, see Sherr and Roberts, 1999). There are two families of CKIs, the Cip/Kip family that currently includes $p21^{Cip1}$, $p27^{Kip1}$, and $p57^{Kip2}$, and the Ink4 family that includes $p16^{Ink4a}$, $p15^{Ink4b}$, $p18^{Ink4c}$, and $p19^{Ink4d}$. Members of both families are tissue and cell type specifically expressed and, in addition to their role in governing cell cycle transitions, have been shown to play an important role in the maintenance of the postmitotic state of numerous cell types (for review, see Vidal and Koff, 2000; Cunningham and Roussel, 2001). Mice harboring a homozygous mutation in $p19^{Ink4d}$ are fertile despite their testicular atrophy (Zindy et al., 2000), but they suffer from a progressive hearing loss that is caused by sporadic cell cycle reactivation in normally postmitotic HCs, followed by cell death (Chen et al., 2003). This process begins toward the end of the first postnatal week and progresses slowly, with only a few auditory HCs observed to reenter the cell cycle at any given time. The mild phenotype of HCs of $p19^{Ink4d-/-}$ mice suggests that other CKIs may act redundantly to inhibit proliferation, as is the case in other cell types (Zindy et al., 1999; Cunningham et al., 2002).

In contrast, inactivation of the retinoblastoma gene (*Rb*) in

Received Aug. 15, 2006; revised Dec. 22, 2006; accepted Dec. 22, 2006.

This work was supported by the following: Academy of Finland, Sigrid Jusélius Foundation, and the European Commission FP6 Integrated Project EuroHear (U.P.); National Institutes of Health (NIH) Grants CA-71907 and CA-90832 and grants from the Children's Brain Tumor Foundation and the American–Lebanese Syrian Associated Charities of St. Jude Children's Research Hospital (M.F.R); and NIH Grant DC-007173 (N.S.). We are grateful to Maria von Numers, Juan Llamos, Welly Makmurra, and Sheri Juntilla for technical assistance and Frederique Zindy for providing the $p19^{Ink4d}$ knock-out mice.

Correspondence should be addressed to Ulla Pirvola, Institute of Biotechnology, University of Helsinki, P.O. Box 56, Viikinkaari 9, 00014 Helsinki, Finland. E-mail: ulla.pirvola@helsinki.fi.

DOI:10.1523/JNEUROSCI.4956-06.2007

 0270-6474/07/271434-11$15.00/0

the inner ear leads to an apparent complete loss of control of the postmitotic state of HCs (Mantela et al., 2005; Sage et al., 2005, 2006). The retinoblastoma protein (pRb) functions as a master switch for the G_1/S-phase transition of the cell cycle and is regulated primarily through modulation of its phosphorylation state (Weinberg, 1995). In its dephosphorylated state, pRb acts as a cell cycle inhibitor, whereas in its phosphorylated state, pRb promotes cell cycle progression. Phosphorylation of Rb is primarily a function of CDK4/6 and CDK2 activity, thus linking the activation of pRb directly to the regulation of CDKs. This leads to the working hypothesis that active inhibition of CDK activity, through the action of CKIs, is required to keep pRb in an inactive state to maintain the postmitotic state of numerous cell types, including HCs.

The more extreme loss of control of the postmitotic state observed in the *Rb* mutant mice (Mantela et al., 2005; Sage et al., 2005, 2006) compared with the $p19^{Ink4d-/-}$ mice (Chen et al., 2003) suggests that additional CKIs may be involved in limiting CDK activity and thus in maintaining the postmitotic state of HCs. It has been shown that $p21^{Cip1}$ is expressed in HCs, but its inactivation does not lead to an altered HC phenotype (Mantela et al., 2005). Here we show that $p21^{Cip1}$ collaborates with $p19^{Ink4d}$ in preventing cell cycle reentry of auditory HCs. The $p19^{Ink4d}/p21^{Cip1}$ double-deficient mice (hereafter termed dko mice) show a much more extreme cell cycle phenotype relative to the $p19^{Ink4d}$ single-null mutant mice, evident as a strong induction of proliferation and subsequent massive HC death occurring during early postnatal life. We also investigate the mechanism of HC apoptosis and show that it involves replicative stress downstream from the onset of cell cycle reentry, including activation of a DNA damage response pathway and the p53 tumor suppressor. Our results suggest that stimulation of proliferation of auditory HCs by suppressing CKI expression *in situ* is unlikely to be a valid approach for their regeneration.

Materials and Methods

Mice. Mouse strains deficient for $p19^{Ink4d}$ (on a 129/SvJ × C57BL/6 × CD-1 mixed background) (Zindy et al., 2000; Chen et al., 2003) and $p21^{Cip1}$ (129S2/SvPas) (Brugarolas et al., 1995) (obtained from The Jackson Laboratory, Bar Harbor, ME) were described previously. The two strains were intercrossed to generate $p19^{Ink4d}/p21^{Cip1}$ dko animals. Genotyping by PCR using DNA extracts from tails was performed as described previously (Brugarolas et al., 1995; Zindy et al., 2000). $p19^{Ink4d}$ and $p21^{Cip1}$ single-null mutant, $p19^{Ink4d}/p21^{Cip1}$ dko, and wild-type mice from the same litters were used for phenotypic analysis. The mouse atonal homolog 1–green fluorescent protein (*Math1–GFP*) transgenic mouse strain used for purification of HCs by fluorescence-activated cell sorting (FACS) was described previously (Doetzlhofer et al., 2004). For timed pregnancies, the morning of vaginal plug identification was taken as E0.5. Animal care was in accordance with institutional guidelines.

Tissue preparation and immunohistochemistry on sections. Inner ears were dissected from dko and wild-type littermates and histologically analyzed at E16.5, at each day between postnatal day 0 (P0) and P7, at P10, P15, and P25, and at 8 weeks of age. Six to 13 mutant ears were analyzed per age. In addition, $p19^{Ink4d}$ single-null mice from the same litters were histologically analyzed at P6 and P7. Dissected specimens were fixed overnight in 4% paraformaldehyde (PFA) in PBS, pH 7.2. Before immersion in PFA, inner ears from P10 and older mice were perilymphatically perfused. Inner ears from P3 and older animals were decalcified in 0.5 M EDTA. Specimens were embedded to paraffin and cut to 5-μm-thick sections that were stained with hematoxylin or antibodies. Epitopes were unmasked by microwave heating (800 W) in 10 mM citrate buffer, pH 6.0, for 10 min. An overnight incubation with the following primary antibodies was performed: polyclonal myosin VIIa (kindly provided by T. Hasson, University of California at San Diego, La Jolla, CA); polyclonal prospero-related homeobox 1(Prox1) (Covance, Princeton, NJ); monoclonal proliferating cell nuclear antigen (PCNA) (Lab Vision, Fremont, CA); monoclonal Ki-67 and polyclonal p53 (Novocastra, Newcastle, UK); rat monoclonal $p19^{Arf}$, monoclonal and polyclonal phospho-H2AX, monoclonal phospho-ataxia telangiectasia mutated (ATM), and polyclonal cyclin E (Upstate Biotechnology, Lace Placid, NY); and rabbit monoclonal cleaved caspase 3, polyclonal phospho-histone H3, phospho-p53, and phospho-checkpoint kinase 2 (Chk2) (Cell Signaling Technology, Beverly, MA). Detection was done with the Vectastain Elite kit or Vectastain Mouse-On-Mouse kit and diaminobenzidine substrate (Vector Laboratories, Burlingame, CA). Sections were counterstained with methyl green. In double-labeling experiments, Alexa 488- and 568-coupled secondary antibodies (Invitrogen, Carlsbad, CA) were used for detection and Vectashield (Vector Laboratories) for mounting. Images were acquired through a CCD camera (DP70; Olympus Optical, Tokyo, Japan) on a microscope (BX61; Olympus Optical) and analySIS software (Olympus Optical).

Semithin sections. Inner ears were dissected from dko and wild-type mice at P6 and fixed overnight in 2.5% glutaraldehyde in 0.1 M phosphate buffer at pH 7.4. Specimens were postfixed in 1% osmium tetroxide and embedded in Epon (Electron Microscopy Sciences, Fort Washington, PA). Sections were cut at 0.5 μm, stained with 2% toluidine blue, and viewed under bright-field optics with the BX61 microscope.

Cochlear whole mounts. Cochlear ducts were dissected from dko and wild-type mice at P7. Tectorial membrane was removed, and specimens were fixed in PFA overnight. Whole mounts were incubated overnight with the antibody to myosin VIIa in PBS containing 5% normal goat serum, 1% bovine serum albumin, and 0.25% Triton X-100, followed by incubation in Alexa 568-coupled secondary antibody. Vectashield was used for mounting. Images were acquired with a TSC SP2 AOBS confocal microscope (Leica, Wetzlar, Germany) using HC PLAPO 20×/0.7 Imm Corr (glycerol) objective. Three-dimensional image stacks were processed and analyzed using the Imaris 4 software (Bitplane, Saint Paul, MN). Stacks were deconvoluted using AutoQuant X software (AutoQuant Imaging, Troy, NY).

Cochleograms. Cochleas dissected from dko, $p19^{Ink4d}$ single-null mutant, and wild-type mice at 8 weeks of age were perilymphatically fixed in 2.5% glutaraldehyde and immersed in the fixative overnight. Specimens were postfixed in 1% osmium tetroxide, embedded in Epon, and processed for surface preparations as described previously (Ylikoski, 1974; Pirvola et al., 2000). Hair cell counts were made under Nomarski optics using the BX61 microscope. Hair cells were characterized as missing if no nucleus at the appropriate location was observed. For cell counting, a 10 × 10 square eye reticular and 40× objective lens were used. The percentage of missing HCs was plotted as a function of the length (in millimeters) of the organ of Corti. Student's *t* test was used for statistical analysis.

Quantitative PCR. After decapitation, mouse embryos and pups were screened for GFP fluorescence. Cochlear tissue obtained from E17.5 to P4 mice were collected and dissected in calcium- and magnesium-free PBS (Invitrogen). Tissue obtained from stage P7 pups was collected and dissected in mammalian Ringer's solution (in mM: 142 NaCl, 5.4 KCl, 1.5 $MgCl_2$, 2 $CaCl_2$, and 10 HEPES, pH 7.2) to maintain epithelial integrity during dissection. Cochlear tissue was reduced to single cells using trypsin (0.05%; Sigma, St. Louis, MO). Hair cells positive for Math1–GFP were FACS purified using a MoFlo cell sorter (DakoCytomation, Glostrup, Denmark). Purity of isolated HCs was assayed by plating and counting the fraction of Math1–GFP-positive cells in the total population. Only isolates >90% pure were used in the final analysis.

Total RNA was isolated from FACS-purified cell samples consisting of ~5000 cells each, using RNeasy Micro kit (Qiagen, Valencia, CA). To improve yield, carrier RNA was added to cell lysates. cDNA was made using Taqman Reverse Transcription Reagents (Applied Biosystems, Foster City, CA). Real-time PCR was performed with Master SYBR Green kit (Applied Biosystems) and gene-specific primer sets on 7500 Real-time PCR Detection System (Applied Biosystems). Each PCR reaction was performed in triplicate. Relative quantification of gene expression was analyzed using the $2(-\Delta\Delta C(T))$ method (Livak and Schmittgen, 2001). cDNA obtained from Math1–GFP-positive stage E17.5 was

used as calibrator, and a ribosomal gene (L19) was used as endogenous reference. After each run, melting curves of reaction products were analyzed to validate specificity of reaction product. PCR primer sets were selected using PrimerExpress 2.0 software (Applied Biosystems) to fit standardized PCR parameters of a 60°C anneal/extension step in SYBR Green Master Mix. PCR primer sets used in these experiments are as follows (F, forward; R, reverse): P21-F, TTCCGCACAGGAGCAAAGT; P21-R, CGGCGCAACTGCTCACT; P19-F, CGGTATCCACTATGCTTCTGGAA; P19-R, CCGCTGCGCCACTCA; p57-F, CAGCGGACGATGGAAGAACT; p57-R, CTCCGGTTCCTGCTACATGAA; p27-F, GCAGGAGAGCCAGGATGTCA; p27-R, CCTGGACACTGCTCCGCTAA; L19-F, GGTCTGGTTGGATCCCAATG; and L19-R, CCCGGGAATGGACAGTCA.

Cells and transfections. HeLa cells were transfected by lipofection with cyclin E–pRC–cytomegalovirus expression vector, incubated for 24 h, fixed, and stained for cyclin E as described by Zhang et al. (2002).

Results

Codeletion of $p19^{Ink4d}$ and $p21^{Cip1}$ leads to S-phase reentry of hair cells at a precise time in early postnatal life

Previous results have shown that $p19^{Ink4d}$ and $p21^{Cip1}$ are expressed in auditory HCs (Chen et al., 2003; Mantela et al., 2005). Mutation of $p19^{Ink4d}$ alone leads to an inner ear phenotype in which, starting at the end of the first postnatal week, a small but progressive number of auditory HCs undergo a loss of control of the postmitotic state that ultimately leads to cell death. This cellular loss caused by aberrant S-phase reentry progresses slowly and leads to severe hearing deficit (Chen et al., 2003). In contrast, inactivation of $p21^{Cip1}$ has no effect on the nonproliferative state of HCs (Mantela et al., 2005). To test the hypothesis that $p19^{Ink4d}$ and $p21^{Cip1}$ cooperate to maintain the postmitotic state of auditory HCs, we crossed the respective knock-out mouse lines and generated dko mice. The double inactivation did not impair viability. At all stages analyzed (E16.5 to adulthood), the gross structure of the cochlear duct and vestibular organs (saccule, utricle, and ampullae) and the associated semicircular ducts was comparable in the dko and wild-type animals (Fig. 1, compare *a*, *b*), indicating that inner ear morphogenesis is not affected by this codeletion.

We first studied the morphology and cell cycle status of auditory HCs at birth in each of the two single-null mutants and in the dko mice ($n = 4$ cochleas of each mutant mouse line). Immunostaining with antibodies to myosin VIIa, a cytoplasmic HC marker (Hasson et al., 1997), and to the homeodomain transcription factor Prox1, which marks two types of supporting cells (Deiter's and pillar cells) adjacent to HCs (Bermingham-McDonogh et al., 2006), showed that the cytoarchitecture of the organ of Corti was comparable with controls in the single- and double-mutant mouse lines (data not shown). Precursor cells of the organ of Corti undergo terminal divisions during midembryogenesis, and differentiating and mature HCs do not proliferate (Ruben, 1967). Similar to wild-type specimens, HCs from either the $p19^{Ink4d}$ and $p21^{Cip1}$ single-null mutant or from the dko mice at P1 were not stained by an antibody to PCNA, which reacts intensely with S-phase nuclei (Fig. 1, compare *c*, *d–f*). We conclude that these mutations do not impair the postmitotic state of auditory HCs at birth or before it.

However, as assessed by PCNA staining of cochleas dissected on consecutive days, HCs from the dko mice ($n = 6$ cochleas), but not from wild-type animals ($n = 6$ cochleas), abruptly reentered S-phase starting at P3 (Fig. 2*a*,*b*). At this early time point, low numbers of PCNA-positive HCs were found, but their numbers significantly increased by P6 ($n = 15$ cochleas) (Fig. 2*c*,*d*). PCNA staining revealed that a large percentage of both types of

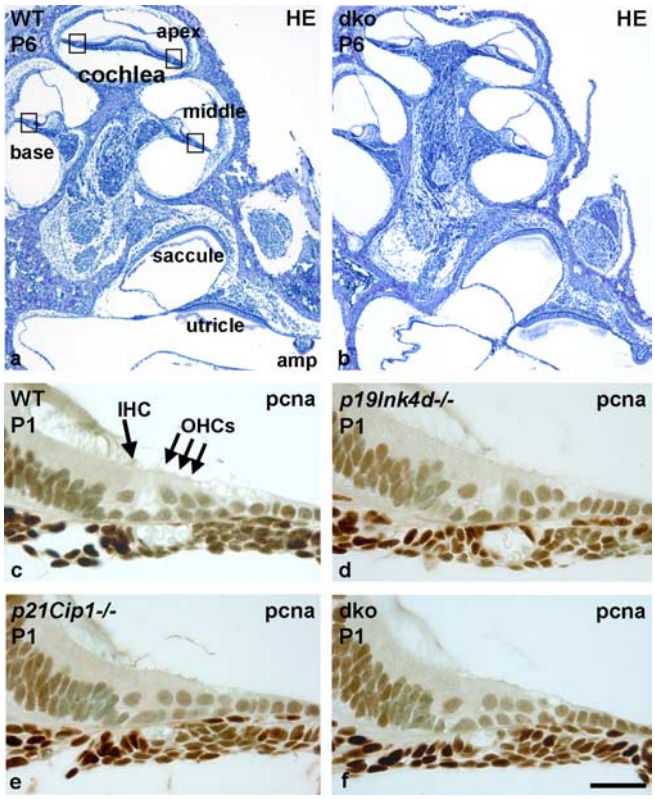

Figure 1. ***a***, ***b***, Codeletion of $p19^{Ink4d}$ and $p21^{Cip1}$ does not alter the gross morphology of the inner ear as shown by hematoxylin-stained sections from the wild-type and dko mice. Boxed areas mark the organ of Corti. ***c–f***, Auditory HCs from the $p19^{Ink4d}$ and $p21^{Cip1}$ single-null mutant and $p19^{Ink4d}/p21^{Cip1}$ dko mice are postmitotic at P1, as shown by the absence of PCNA immunoreactivity. amp, Ampulla. Scale bar (in ***f***): ***a***, ***b***, 200 μm; ***d–f***, 40 μm.

auditory HCs, the inner and outer hair cells (IHCs and OHCs), were undergoing DNA replication, although proportionally more IHCs showed this activity. Abnormal DNA replication continued at P10 ($n = 10$ cochleas) (Fig. 2*e*,*f*), but it rapidly declined thereafter, so that only a few PCNA-positive cells were found at P16 ($n = 6$ cochleas) and P25 ($n = 5$ cochleas), as shown quantitatively in Figure 2*g*. Of note, we also counted the numbers of PCNA-positive HCs in the $p19^{Ink4d}$ single-null mutant mice at P6 and found that the extent of S-phase reentry was significantly less than in the age-matched dko mice ($p < 0.001$ for both IHCs and OHCs) (Fig. 2*g*). Together, these data show that the concurrent deletion of $p19^{Ink4d}$ and $p21^{Cip1}$ triggers high-level induction of DNA replication in auditory HCs during a restricted period of early postnatal development and that there is a synergy between $p19^{Ink4d}$ and $p21^{Cip1}$ in the maintenance of growth arrest. As measured by PCNA staining, the double mutation did not affect the postmitotic status of supporting cells of the organ of Corti (Fig. 2*b*,*d*,*f*)

S-phase reentry of hair cells is followed by mitosis and death

We next assessed whether HCs that have reentered the cell cycle can progress into mitosis and divide. Sections were stained with an antibody to phospho-histone H3, which marks cells in late G_2-phase (patchy staining) and M-phase (condensed staining) (Hendzel et al., 1997). In contrast to wild-type animals, cochleas from the dko mice contained immunopositive HCs between P3 and P10, most abundantly at P6 and P7. Condensed phosphohistone H3 staining was mostly seen in IHCs, whereas most of the immunoreactive OHCs were in G_2 based on the patchy staining

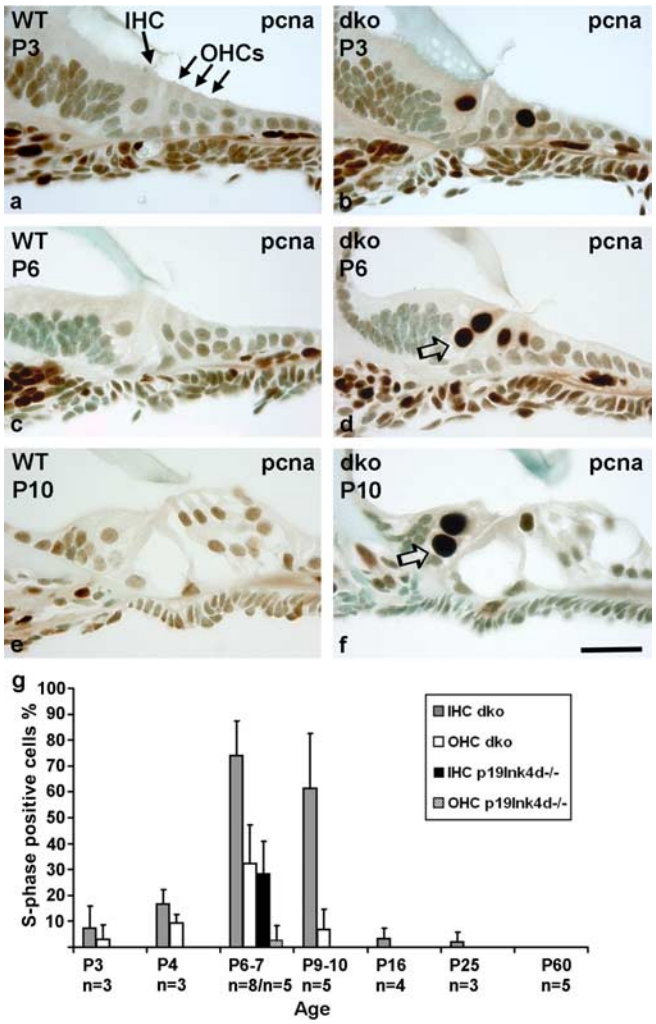

Figure 2. Codeletion of $p19^{Ink4d}$ and $p21^{Cip1}$ leads to the abrogation of the postmitotic state of auditory HCs at perinatal life. ***a***, ***b***, Induction of PCNA immunoreactivity at P3 marks the onset of S-phase reentry of auditory HCs from the dko mice, in contrast to wild-type controls. ***c***, ***d***, At P6, large part of IHCs and OHCs from the dko mice stain positively for PCNA. Supernumerary IHCs can be seen (open arrow). ***e***, ***f***, Several HCs show PCNA positivity still at P10. Note also the presence of supernumerary IHCs (open arrow) and the loss of part of OHCs at this stage. Supporting cells adjacent to HCs do not proliferate at any stage. ***g***, Quantification of IHCs and OHCs undergoing DNA replication at different postnatal ages, as assessed by counting the numbers of PCNA-positive cells from 12 midmodiolar sections per cochlea. Numbers of positive cells are expressed as percentage of total numbers of HCs in these sections. Values represent mean ± SD. Data are from three to eight cochleas per age. Wild-type mice do not show PCNA-positive HCs (data not shown). PCNA-immunoreactive HCs were also counted from the cochleas of $p19^{Ink4d}$ single-null mice at P6 and P7. Note the large difference in the extent of DNA replication between the single-null and dko mice. Scale bar (in ***f***): ***a–f***, 40 μm.

pattern (Fig. 3, compare *a*, *b*). The numbers of PCNA-stained HCs clearly surpassed those of phospho-histone H3-positive HCs (data not shown). Although the organ of Corti was not obviously hyperplastic, sections immunostained for myosin showed an excess of IHCs, indicative of successful divisions and of the fact that the extra cells had molecular characteristics of HCs (Fig. 3, compare *c* with *d*,*e*). Also, supernumerary HCs showed PCNA immunoreactivity (Fig. 2*d*,*f*). However, some IHCs showed an abnormal nuclear morphology, suggesting that the codeletion of $p19^{Ink4d}$ and $p21^{Cip1}$ led to polyploidy at a low frequency (Fig. 3*d*).

The organ of Corti from the dko mice displayed a normal complement of supporting cells, as evidenced by a comparable expression of Prox1 in the mutant and control animals (Fig. 3, compare *f*, *g*). These results, together with the lack of PCNA and phospho-histone H3 staining in the supporting cell layer (compare Figs. 2*b*,*d*,*f*, 3*b*) suggested that the postmitotic state of these nonsensory cells was not abolished by the codeletion of $p19^{Ink4d}$ and $p21^{Cip1}$.

The onset of abnormal proliferation of auditory HCs from the dko mice preceded the loss of HCs. First signs of HC loss were seen at P6, and the loss rapidly progressed thereafter, based on the clear differences in the histology of the organ of Corti between P6 and P10 (Fig. 2, compare *d*, *f*). Observations of cleaved caspase 3 positivity suggest that both IHCs and OHCs died through apoptosis (Fig. 3, compare *h*, *i*). Of note, the dko mice showed normal developmental apoptosis in the precursor-like cells of the greater epithelial ridge (GER) (Nikolic et al., 2000), the area located medially to the organ of Corti (Fig. 3, compare *h*, *i*). Together, these results show that S-phase reentry of HCs in response to the $p19^{Ink4d}/p21^{Cip1}$ codeletion rapidly leads to apoptosis.

To obtain a better resolution of cytological abnormalities in the organ of Corti from the dko mice, we analyzed plastic-embedded semithin sections stained with toluidine blue at P6 ($n = 6$ cochleas) (Fig. 3*j–o*). In contrast to wild-type specimens that show one IHC and three OHCs per cochlear half-turn in a cross-section, the dko mice displayed two to four layers of IHCs (Fig. 3, compare *j*, *k*). Several sections showed IHCs in mitosis at the lumenal surface (Fig. 3*k*), but only a few OHCs undergoing division were found (Fig. 3*l*). Also, IHCs with two separate nuclei or one bi-lobed or multi-lobed nucleus and decondensed chromatin were found, suggesting failures at the level of the cleavage furrow and cytokinesis (Fig. 3*m*). Both IHCs undergoing mitosis and IHCs with aberrant nuclear morphologies carried stereociliary bundles at the lumenal surface (Fig. 3, compare *j* with *k*,*m*), but many of the more deeply located supernumerary IHCs did not appear to extend a proper mechanosensory domain to the epithelial surface (Fig. 3*k*,*m*). Consistent with the findings made in paraffin sections, semithin sections showed profiles of IHCs and especially of OHCs with distinct nuclear condensations typical of apoptotic cells (Fig. 3*n*,*o*).

Codeletion of $p19^{Ink4d}$ and $p21^{Cip1}$ leads to the destruction of the organ of Corti

We next quantified auditory HC loss in the dko mice and compared it with the loss seen in the $p19^{Ink4d-/-}$ animals (Fig. 4*a–f*). Mutation of $p19^{Ink4d}$ leads to a progressive auditory HC loss, such that no loss was observed in the knock-out mice at P5, but, by 7 weeks of age, a loss of 43% of IHCs and 15% of OHCs was found in the basal region of the cochlea (Chen et al., 2003). In that study, HC loss in other regions of the cochlea was not studied. We counted the numbers of lost HCs throughout the length of the cochlear duct in whole mounts from 2-month-old $p19^{Ink4d-/-}$ mice ($n = 4$ cochleas), which were littermates of the $p19^{Ink4d}/p21^{Cip1}$ dko animals. Consistent with Chen et al. (2003), we found that the basal and middle regions of the cochlea were affected by the $p19^{Ink4d}$ single inactivation, with a loss of 29% of IHCs and 9% of OHCs (0–4 mm). This loss of IHCs was significant ($p < 0.01$). Only minor HC loss was seen at upper levels of cochleas (Fig. 4*f*).

In contrast to mice lacking $p19^{Ink4d}$ that do not show HC loss at P5 (Chen et al., 2003), 2.5% of IHCs and 5% of OHCs were lost in the dko mice at P7, as assessed from myosin-stained cochlear whole mounts ($n = 6$) (Fig. 4*a*,*b*). In a pattern similar to that observed for abnormal proliferation, HC loss was concentrated to the upper basal-to-middle region of the cochlea (data not shown). The fact that the dko mice survived to adulthood allowed us to study whether progressive HC loss is a part of the altered phenotype in the dko mice, as shown previously in the $p19^{Ink4d}$

single-null mutant mice (Chen et al., 2003). At 2 months of age, paraffin sections showed a severe HC loss, but surviving HCs were negative for PCNA, phospho-histone H3, and cleaved caspase 3, similar to controls (data not shown). Consistent with sectioned material, plastic-embedded cochlear whole mounts (cochleograms; $n = 4$) (Fig. 4, compare *c*, *d*) at 2 months of age showed a severe depletion of HCs in the basal and middle regions of cochleas. Quantification of HC loss in cochleograms (Fig. 4*e*) showed that the middle region of the cochlea (2–4 mm from the round window) was most severely affected, with a loss of 66% of IHCs and 87% of OHCs. In the basal region (0–2 mm), these values were 64% and 62%, respectively. The best cellular preservation was seen in the apical region (4–6 mm) in which only 26% of IHCs and 26% of OHCs were lost. In the basal and middle regions (0–4 mm), the loss of both IHCs and OHCs was significant ($p < 0.001$). Together, the cochlear phenotype of mice lacking $p19^{Ink4d}$ was profoundly exacerbated by the simultaneous inactivation of $p21^{Cip1}$. In addition, the timing of HC loss in the dko mice parallels the timing of cell cycle reentry, suggesting strongly that abnormal proliferation was rapidly followed by apoptosis in HCs within specific regions along the length of the cochlear duct.

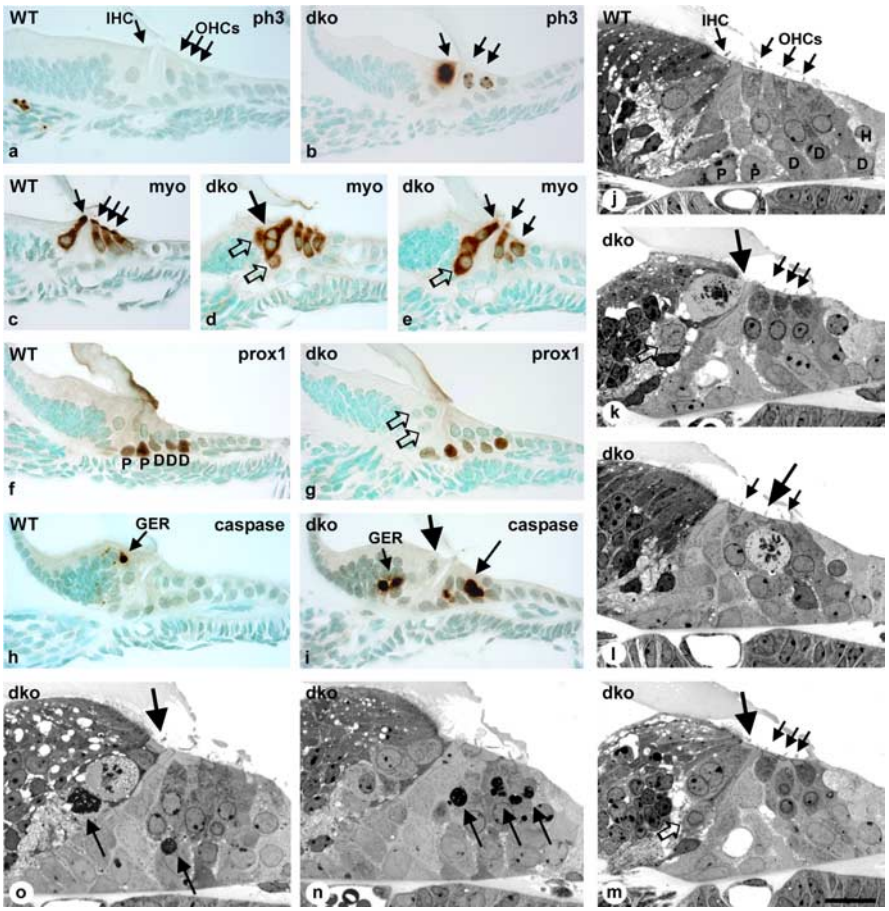

Figure 3. Codeletion of $p19^{Ink4d}$ and $p21^{Cip1}$ leads to abnormal cell divisions and death of auditory HCs. Paraffin-embedded (***a–i***) and plastic-embedded semithin (***j–o***) sections through the organ of Corti at P6. ***a***, ***b***, In contrast to the wild-type specimen, the section from a dko mouse shows a phospho-histone H3-stained IHC undergoing mitosis (condensed staining) and two OHCs in G_2-phase (patchy staining). ***c–e***, In contrast to wild-type specimens, myosin-stained sections showed an increase in IHC numbers (open arrows mark supernumerary IHCs). Also, a binuclear IHC is seen (large arrow in ***d***) and loss of part of OHCs (***e***). ***f***, ***g***, Prox1-immunoreactive Deiter's and pillar cells are unaffected in the dko mice. ***h***, ***i***, Cleaved caspase 3 immunostaining (arrows) reveals normal developmental apoptosis in the greater epithelial ridge of both the wild-type and dko mice. This staining is also seen in the OHC region from the dko mouse. Note a mitotic IHC (large arrow) in the dko specimen. ***j–l***, In contrast to wild-type animals (***j***), semithin sections prepared from the dko mice show mostly IHCs (***k***, large arrow) but also a few OHCs (***l***, large arrow) in mitosis. Note an extra IHC (open arrow in ***k***) below the mitotic IHC. ***m***, A binuclear IHC with decondensed DNA (large arrow) at the lumenal surface and an underlying supernumerary IHC (open arrow). ***n***, ***o***, The organ of Corti from the dko mice reveals several apoptotic IHCs and OHCs (arrows). Note a mitotic IHC at the lumen that shows signs of degeneration (large arrow in ***o***). ph3, Phospho-histone H3; myo, myosin VIIa; P, pillar cell; D, Deiter's cell; caspase, cleaved caspase-3; H, Hensen cell. Scale bar (in ***f***): ***a–i***, 60 μm; ***j–o***, 20 μm.

CKI levels vary independently during the postnatal period of hair cell maturation

The loss of both $p19^{Ink4d}$ and $p21^{Cip1}$ could reveal additional redundancy among the remaining CKIs, acting to maintain the postmitotic state of HCs before the onset of proliferation at P3 and/or at mature stages, after the cessation of abnormal proliferation. Regardless, normal, developmentally regulated changes in the levels of CKIs during the early postnatal period of HC maturation are likely to influence the sensitivity of HCs to disruptions of the postmitotic state. To study the expression of *CKIs* during this period, HCs harboring the GFP under the control of a *Math1* (*Atoh1*, for atonal homolog 1) enhancer were purified by FACS (Doetzlhofer et al., 2004) from E17.5, P0, P2, P4, and P7 cochlea, and *CKI* expression was analyzed by quantitative PCR (Fig. 5). From E17.5 to P7, we observed an overall increase of 2.5- to 4-fold in the level of expression of $p19^{Ink4d}$, $p21^{Cip1}$, and $p27^{Kip1}$. In the case of $p19^{Ink4d}$, there was an abrupt twofold increase between E17.5 and P0 and another between P4 and P7, whereas the increase of $p21^{Cip1}$ was more gradual and began only at approximately P4. Interestingly, $p27^{Kip1}$, which is not detected in differentiated HCs by immunohistochemistry (Chen and Segil, 1999; Lowenheim et al., 1999), was detected at low levels in HCs around birth, and this low level increased by fourfold between P4 and P7. In support of this observation, genetic evidence suggests a role for $p27^{Kip1}$ in the maintenance of the postmitotic state of differentiated HCs (N. Segil and A. Doetzlhofer, unpublished data). $p57^{Kip2}$ was expressed in HCs at E17.5 and P0 but, in contrast to other *CKIs*, showed a marked downregulation by P4 (Fig. 5). Other members of the Ink4d family, $p16^{Ink4a}$, $p15^{Ink4b}$, and $p18^{Ink4c}$, were not detected at any stages assayed (data not shown). These data indicate that the levels of *CKI* mRNA vary independently during the period of postnatal maturation of HCs. In addition, the rising *CKI* levels during the early postnatal period correlate with the fact that aberrant HC proliferation was a short-lived event, with the main part of it being over by the third postnatal week (Figs. 2, 5).

Abnormal proliferation of hair cells precedes the activation of DNA damage response and p53-dependent apoptosis

We sought to determine the molecular pathway(s) leading to apoptosis of HCs with abnormal proliferation. The tumor sup-

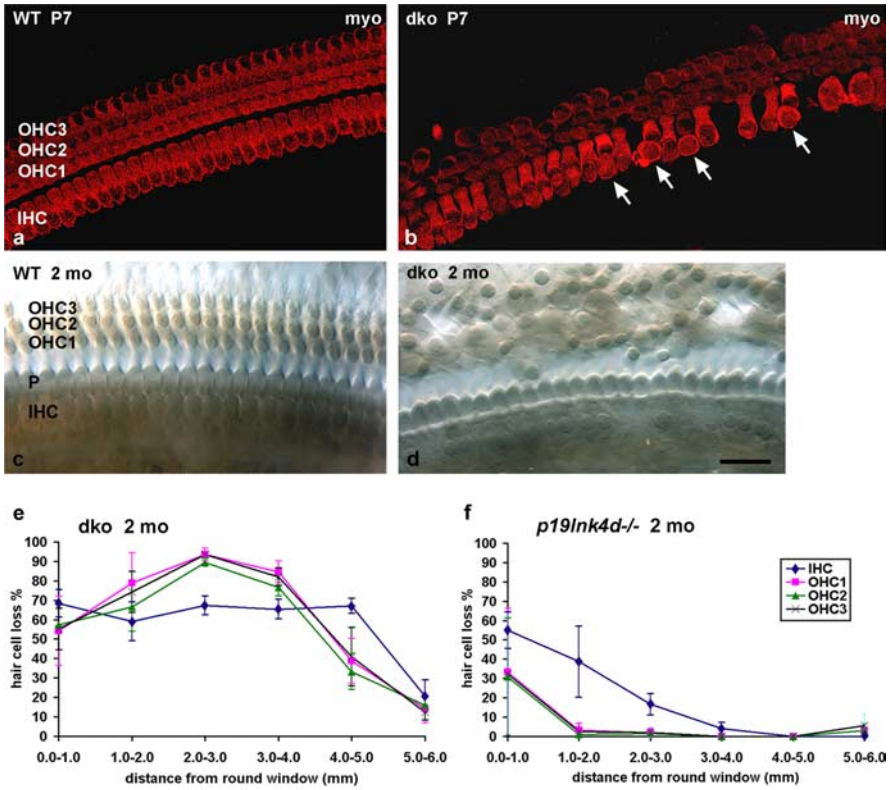

Figure 4. Codeletion of $p19^{Ink4d}$ and $p21^{Cip1}$ leads to the loss of auditory HCs in a spatiotemporally distinct pattern. ***a***, ***b***, At P7, a myosin-stained whole mount prepared from a wild-type cochlea shows one row of IHCs and three rows of OHCs. In contrast, a whole mount prepared from the middle region of the cochlea from a dko mouse shows scattered HC loss and an excess of IHC nuclei (arrows). ***c***, ***d***, At 2 months of age, a plastic-embedded whole mount prepared from the middle region of the cochlea from a dko mouse shows severe depletion of HCs. OHCs are almost absent, and many IHCs are lost as well. Many of the nuclei seen in the area of OHCs belong to the scar-forming Deiter's cells. ***e***,***f***, Percentage of HC loss quantified throughout the length of the cochlear duct in the dko (***e***) and $p19^{Ink4d}$ single-null (***f***) mice at 2 months of age. The round window specifies the base of the cochlear duct, which has a length of ~6 mm in the adult mouse. Results show mean ± SD. The dko mice show significant loss of IHCs and OHCs throughout the length of the cochlear duct, but the apical region is clearly less affected than the middle and basal regions ($n = 4$ cochleas). In contrast, $p19^{Ink4d}$single-null mice ($n = 4$ cochleas) show significantly milder HC loss, and it is primarily restricted to the basal region of the cochlea. Of note, OHC loss in the $p19^{Ink4d-/-}$ mice is insignificant relative to the dko animals. P, Pillar cell; myo, myosin VIIa. Scale bar (in ***d***): ***a***, ***b***, 40 μm; ***c***, ***d***, 50 μm.

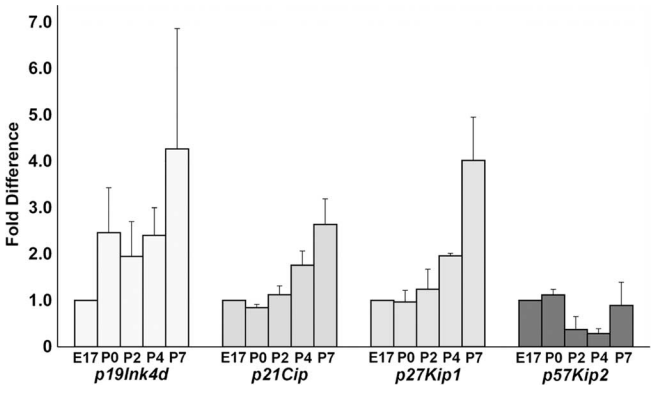

Figure 5. Postnatal changes in the expression of *CKIs* in purified auditory HCs. Quantitative PCR was used to measure the changing levels of individual *CKIs* in late embryogenesis and during the first postnatal week. Expression in E17.5 HCs was set as baseline (1) for each *CKI*, and changes (fold difference) in each *CKI* were plotted over time (P0, P2, P4, P7). Two to three independent samples were measured at each time point (mean ± SEM).

pressor p53 is a critical inducer of apoptosis in cells with deregulated growth in response to several stress signals (for review, see Vousden and Lu, 2002; Zhivotovsky and Kroemer, 2004). The inner ear sensory epithelia of wild-type mice did not show detectable expression of the p53 protein (Fig. 6*a*). In contrast, IHCs and OHCs from the dko animals showed robust p53 induction, as assessed at P6 and P10 by immunostaining with antibodies detecting the p53 protein (Fig. 6*b*) and its activated form (phosphorylation at Ser15) (Fig. 6*c*). In some specimens, p53 induction was directly localized to the areas positive for cleaved caspase 3, as evidenced from adjacent sections (Figs. 4*i*, 6*b*). The nearby supporting cells and the GER (Fig. 6*b*,*c*) as well as the vestibular sensory epithelia from the dko mice were negative for p53 and phospho-p53. These results suggest that p53 plays a proapoptotic role in auditory HCs from the dko animals.

To better understand the activation of p53 in HCs that reenter the cell cycle in the absence of $p19^{Ink4d}$ and $p21^{Cip1}$, we studied the role of the tumor suppressor $p19^{Arf}$, which normally responds to uncontrolled proliferation resulting from oncogenic stimulation and viral transformation rather than from DNA damage. $p19^{Arf}$ promotes p53 activation by binding to the p53-negative regulator Mdm2 (transformed mouse 3T3 cell double minute 2), thereby triggering cell cycle arrest or apoptosis, depending on collateral signals and cell context (for review, see Lowe and Sherr, 2003). We did not find $p19^{Arf}$ expression in the organ of Corti from wild-type (data not shown) or dko (Fig. 6*d*) mice. The embryonic eye, one of the few normal tissues showing $p19^{Arf}$ expression (Zindy et al., 1997, 2003; McKeller et al., 2002; Bertwistle et al., 2004), was used as a positive control (Fig. 6*d*′).

Replicative stress leading to DNA damage stimulates p53-dependent apoptosis (for review, see Zhivotovsky and Kroemer, 2004). We evaluated whether abnormal proliferation of HCs triggered replicative stress and DNA damage by assaying the induction of cyclin E, a marker for replicative stress (Ekholm-Reed et al., 2004; Bartkova et al., 2005). HeLa cells ectopically expressing human cyclin E (Fig. 6*e*′) were used as a positive control. At P6 (Fig. 6, compare *e*, *f*) and P10 (data not shown), cyclin E was not expressed in wild-type HCs but was strongly induced in mutant cells from the dko mice.

Deregulated replication and double-strand breaks (DSBs) in DNA activate the DNA damage response pathway, including phosphorylation of histone H2AX, ATM kinase, and Chk2 (for review, see Kastan and Bartek, 2004). Prominent phospho-H2AX immunostaining (phosphorylation at Ser139), marking the foci of DSBs, was observed in several IHC and OHC nuclei from the dko mice at P6 (Fig. 6, compare *g*, *h*). Phosphorylation of ATM and Chk2 links the formation of DSBs to p53 induction (for review, see Kastan and Bartek, 2004). Auditory HCs from the dko mice showed immunostaining for activated ATM (phosphorylation at Ser1981) and Chk2 (phosphorylation at Thr68), in contrast to wild-type animals (Fig. 6, compare *i* with *j* and *k* with *l*). Cochlear supporting cells (Fig. 6*j*,*l*) and vestibular sensory epithelia (data not shown) from the dko animals did not react with these markers of DNA damage.

The above results raised the question of temporal relationship between abnormal proliferation, DNA damage response, and apoptosis. The fact that S-phase reentry of HCs from the dko mice was initiated at P3 (Fig. 2*b*) but activation of H2AX, ATM, Chk2, and p53 was not detected before P6 (data not shown) suggested that abnormal proliferation precedes DNA damage and apoptosis. To establish this further, we performed double labeling on paraffin sections at P6, using Ki-67 as an S-phase marker. We first confirmed that, similar to the PCNA antibody (Fig. 2), the antibody against Ki-67 reacted with numerous myosin-positive HCs from the dko mice, in contrast to wild-type animals (Fig. 7*a*,*b*). Based on double-labeling experiments at P6, low levels of phospho-Chk2 were detected in some of Ki-67-positive HCs (data not shown), but the HCs with strong phospho-Chk2 expression were Ki-67 negative (Fig. 7*c*,*d*). These data strongly suggest that S-phase reentry precedes the activation of the DNA damage checkpoint.

Double-labeling experiments were also performed to find out the temporal relationship between activation of a DNA damage response (phospho-ATM or phospho-H2AX) and onset of apoptosis (cleaved caspase 3) (Fig. 7*e–i*). In all cases, numerous HCs positive for phospho-ATM or phospho-H2AX were found in the absence of cleaved caspase 3. Of the low numbers of caspase-positive HCs present (reflecting the fact that apoptosis is a rapid process), the majority showed colocalization with phospho-ATM (Fig. 7*e*,*f*). Caspase-positive HCs also showed phospho-H2AX expression. However, in apoptotic HCs, H2AX activation appeared to be associated with fragmented DNA rather than with the foci of DNA DSBs (Fig. 7*g–i*) (Rogakou et al., 1998). This observation is consistent with recent data showing that, in addition to its involvement in DNA damage, activated H2AX is required for apoptotic DNA fragmentation (Lu et al., 2006). Together, our results strongly suggest that HCs from the dko mice progress from DNA damage, associated with aberrant cell cycle reentry, to apoptosis.

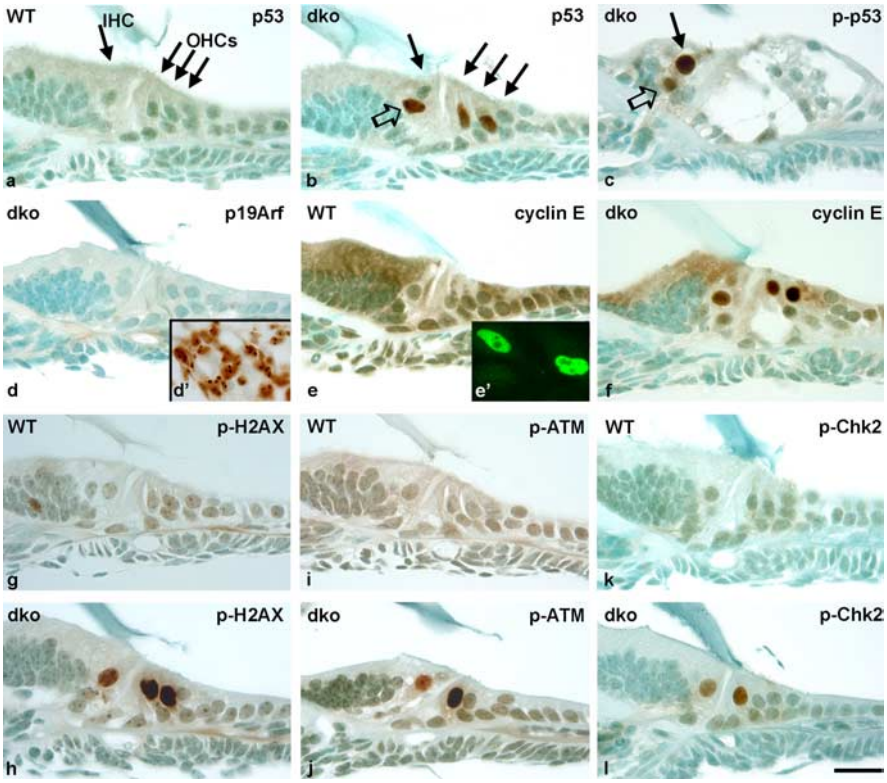

Figure 6. Codeletion of $p19^{Ink4d}$ and $p21^{Cip1}$ triggers a DNA damage response in auditory HCs with abnormal proliferation. ***a***, ***b***, At P6, p53 protein is not expressed in the organ of Corti of wild-type mice but is upregulated in IHCs and OHCs from the dko animals. The open arrow marks a positive supernumerary IHC. ***c***, At P10, HCs from the dko mice show immunostaining for the phosphorylated form of p53. This staining is most prominent in IHCs, including supernumerary IHCs (open arrow), because a large part of OHCs are lost by this age. ***d***, ***d′***, At P6, $p19^{Arf}$ is not expressed in the organ of Corti from the dko mice. The vitreous perivascular cells of the embryonic eye (E15) serve as positive controls. ***e***, ***e′***, ***f***, At P6, in contrast to wild-type specimens, cyclin E immunostaining is seen in auditory HCs from the dko mice. The same antibody stains HeLa cells that ectopically express cyclin E. ***g***, ***h***, At P6, phospho-H2AX immunostaining is undetectable in the organ of Corti from wild-type animals, in contrast to IHCs and OHCs from the dko mice. ***i***, ***j***, At P6, hair cells show activated ATM in the cochleas of the dko but not of wild-type animals. ***k***, ***l***, At P6, phospho-Chk2 induction is seen in IHCs and OHCs from the dko mice, in contrast to wild-type animals. p-p53, Phospho-p53; p-H2AX, phospho-H2AX; p-ATM, phospho-ATM; p-Chk2, phospho-Chk2. Scale bar (in ***j***): ***a–j***, ***d′***, 40 μm; ***e′***, 25 μm.

Mechanisms regulating the maintenance of the postmitotic state of hair cells are sensory organ specific

We next studied whether the cell cycle status of HCs in the vestibular organs is affected in the dko mice, in a manner similar to auditory HCs. Vestibular HCs from the mutant mice at any age (E16.5 to adulthood) did not react with PCNA and phospho-histone H3 antibodies. In addition, myosin and hematoxylin staining showed a normal morphology of these cells (Fig. 8, compare *a–c*, *d–f*). Similar results were obtained with vestibular HCs from the $p19^{Ink4d}$ single-null mutant mice (data not shown). These data suggest that distinct qualitative differences occur at the level of CKIs in the control of the postmitotic state between vestibular and cochlear HCs.

Discussion

Maintenance of the postmitotic state of terminally differentiated cell types is a poorly understood process involving multiple elements of the core cell cycle machinery. In this report, we have shown that the CKIs $p19^{Ink4d}$ and $p21^{Cip1}$ collaborate to maintain the nondividing state of sensory HCs of the organ of Corti. Interestingly, whereas inactivation of $p19^{Ink4d}$ alone leads to a slow but progressive HC loss (Chen et al., 2003) and $p21^{Cip1}$ knock-out mice develop a normal inner ear phenotype (Mantela et al., 2005), codeletion of $p19^{Ink4d}$ and $p21^{Cip1}$ causes a sudden loss of control of the postmitotic state starting at P3, leading to the death of a large part of HCs in early postnatal life (Fig. 2). Surviving HCs do not proliferate in adulthood, an observation that correlates with a general upregulation of *CKI* mRNAs in HCs postnatally (Fig. 5). Inappropriate HC divisions are accompanied by several indicators of replicative stress and by the activation of a DNA damage response pathway, leading to p53-mediated apoptosis. Similar to auditory HCs from the dko mice (present study) and from the $p19^{Ink4d}$ knock-out mice (Chen et al., 2003), cell cycle reentry of HCs has been demonstrated previously in *Rb* mutant mice (Mantela et al., 2005; Sage et al., 2005, 2006), suggesting that CKI-mediated suppression of CDK activity leads to the inactivation of pRb-dependent functions.

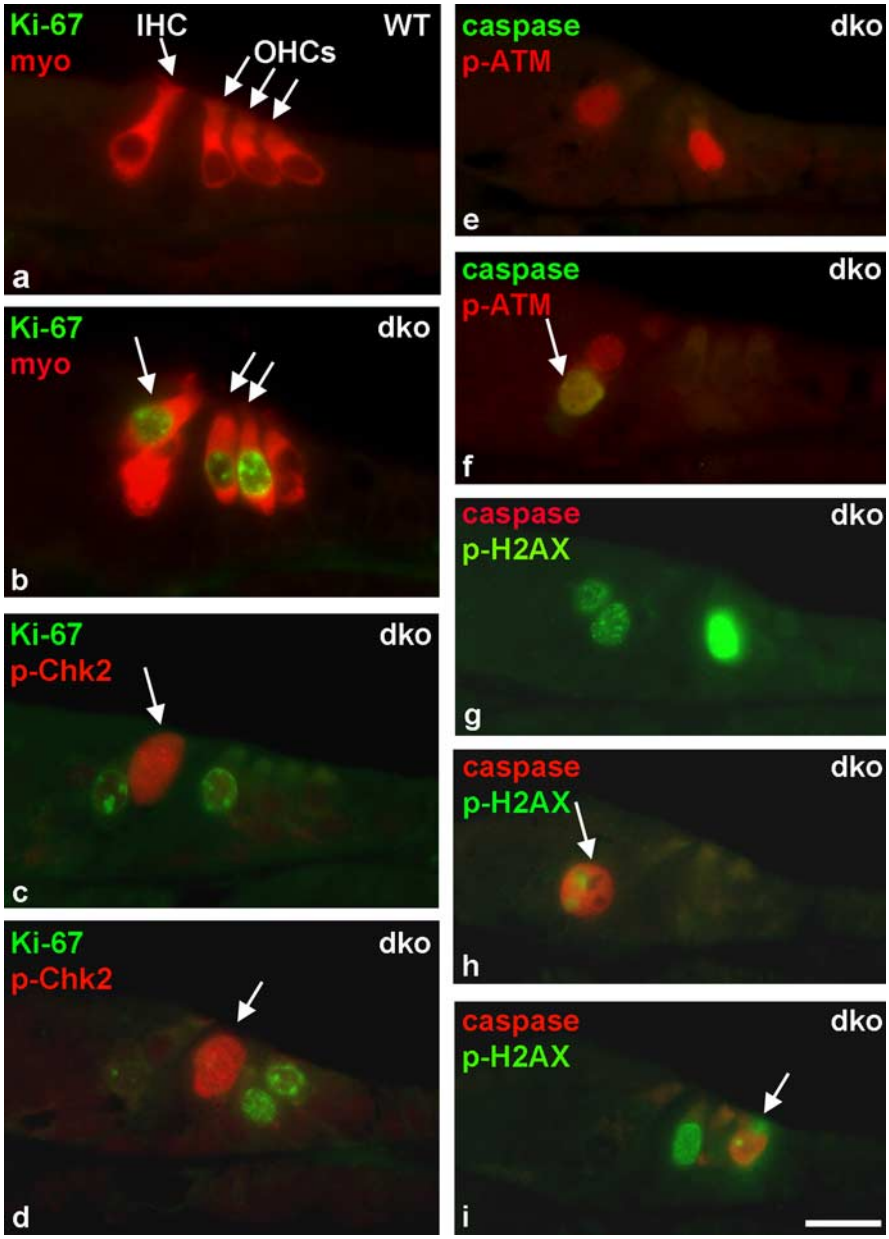

Figure 7. Relationship between abnormal proliferation, DNA damage, and apoptosis in auditory hair cells codeleted for $p19^{Ink4d}$ and $p21^{Cip1}$, as revealed by double labeling at P6. ***a***, ***b***, The proliferation marker Ki-67 is expressed in myosin-positive hair cells in the mutant cochleas, in contrast to wild-type specimens. ***c***, ***d***, The strongly phospho-Chk2-labeled IHC (***c***, arrow) and OHC (***d***, arrow) are not stained for Ki-67. ***e***, ***f***, Most of phospho-ATM-positive hair cells do not show cleaved caspase 3 labeling (***e***). Of the cells expressing this apoptotic marker, the majority coexpress phospho-ATM (***f***, arrow). ***g–i***, Several hair cell nuclei from the mutant cochleas show a distinct granular pattern of phospho-H2AX labeling, and most of them lack cleaved caspase 3 expression (***g***). Apoptotic hair cells (an IHC marked with arrow in ***h***, an OHC marked with arrow in ***i***) show phospho-H2AX staining that is localized to fragmented DNA. myo, Myosin VIIa; p-Chk2, phospho-Chk2; p-ATM, phospho-ATM; p-H2AX, phospho-H2AX; caspase, cleaved caspase 3. Scale bar (in ***i***): ***a–i***, 40 μm.

CKI expression in hair cells during postnatal maturation

Our results show that, during neonatal stages, the maintenance of the postmitotic state of auditory HCs likely depends on the interplay between several CKIs and on their dynamically changing expression patterns (Fig. 5). Both $p19^{Ink4d}$ and $p21^{Cip1}$ were expressed in HCs at E17.5, and their expression subsequently rose by P7. Similarly, $p27^{Kip1}$ and $p57^{Kip2}$ were detected in HCs at late embryogenesis and at birth, but, in the case of $p27^{Kip1}$, levels also rose approximately fourfold, paralleling $p19^{Ink4d}$, whereas $p57^{Kip2}$ levels fell approximately twofold by P4 and then appeared to rise again to embryonic levels, but no increase above embryonic levels was detected. Although functional correlates between these temporal changes in *CKI* levels and the changes in the developmental timing of abnormal proliferation in the dko mice have not been made, the drop in $p57^{Kip2}$ between P0 and P4 may help to explain the abrupt onset of abnormal proliferation at P3. Similarly, the rise in $p27^{Kip1}$ level at P7 might be responsible for the decrease in abnormal proliferation between P7 and P10 (Fig. 2). Thus, in the absence of $p19^{Ink4d}$ and $p21^{Cip1}$, the normal changes in developmental expression of remaining CKIs could render HCs of different ages differentially susceptible to disruptions of the postmitotic state.

It should be noted that we used the $2(-\Delta\Delta C(T))$ method (Livak and Schmittgen, 2001) for calculating mRNA abundance. This method allows for precise relative comparisons of the level of specific mRNA between populations but not between different mRNA species. Thus, although we measured the relative change of each *CKI* over time, we cannot say which, if any, of the *CKI*s predominates in abundance. Indeed, although $p27^{Kip1}$ is readily detected in HCs by this method, we have been previously unable to detect $p27^{Kip1}$ protein in HCs by immunohistochemistry (Chen and Segil, 1999), suggesting that either $p27^{Kip1}$ levels in HCs are extremely low or $p27^{Kip1}$ is being translationally controlled (Hengst and Reed, 1996). Nonetheless, it is possible that low levels of $p27^{Kip1}$ protein are produced and may play a role in the maintenance of the postmitotic state of auditory HCs, as is the case in supporting cells. In any case, our analysis shows a complex pattern of early postnatal regulation of *CKI*s in auditory HCs that, combined with the temporal regulation of HC phenotype in the dko mice, strongly support a role for these molecules in the developmental control of the postmitotic state.

Role of $p21^{Cip1}$ in G_1/S-phase transition and in checkpoint control

The present results showing significantly increased numbers of HCs undergoing DNA synthesis in the dko mice relative to the $p19^{Ink4d}$ single-null mutant animals (Fig. 2) point to an important role of $p21^{Cip1}$ in preventing S-phase reentry, in collaboration with $p19^{Ink4d}$ whose role in this regulation has been shown previously (Chen et al., 2003).

In addition to the regulation of G_1/S-phase transition, $p21^{Cip1}$ is known to be involved in the G_2/M checkpoint. DNA damage leads to p53 activation, which induces apoptosis and/or $p21^{Cip1}$-mediated cell cycle arrest, depending on cell context (for review,

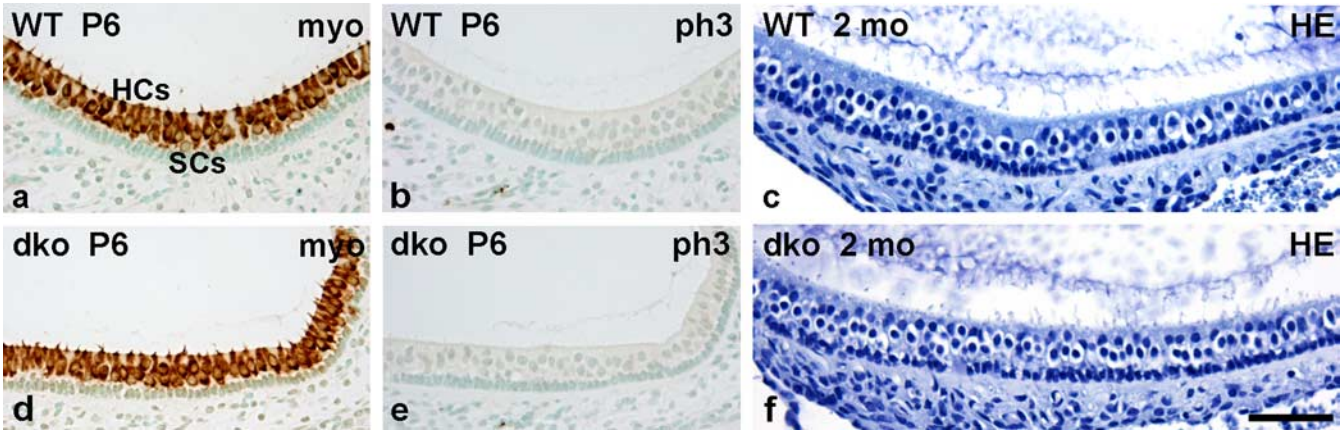

Figure 8. Vestibular HCs are unaffected by the codeletion of $p19^{Ink4d}$ and $p21^{Cip1}$, as revealed in sections through the sensory epithelium of the saccule. ***a***, ***b***, Myosin-stained vestibular HCs are arranged as a lumenal cell layer. They do not show mitotic activity in wild-type specimens, as revealed by phospho-histone H3 immunostaining at P6. ***c***, Hematoxylin-stained section through the saccule from the wild-type ear at adulthood. ***d***, ***e***, Myosin and phospho-histone H3 stainings reveal a normal morphology and a postmitotic status of vestibular HCs from the dko mice at P6. ***f***, Hematoxylin staining shows a normal morphology of the saccule from the adult dko mouse. myo, Myosin VIIa; SC, supporting cell; ph3, phospho-histone H3; HE, hematoxylin. Scale bar (in ***f***): ***a–f***, 80 μm.

see Vousden and Lu, 2002; Zhivotovsky and Kroemer, 2004). *In vitro* studies have shown that DNA damage does not lead to an arrest of cells deficient for $p21^{Cip1}$; rather, these cells progress into mitosis but show failures in cytokinesis (Bunz et al., 1998; Niculescu et al., 1998). Our results show that S-phase reentry of auditory HCs from the dko mice was followed by DNA damage and p53 activation, and, analogously to the cell-based studies, the lack of $p21^{Cip1}$ may explain why a part of auditory HCs escaped from G_2 arrest and progressed into mitosis. The codeletion of $p19^{Ink4d}$ and $p21^{Cip1}$ generated supernumerary HCs but also HCs with mitotic abnormalities, resulting in binuclear cells or in cells with a single bi-lobed or multi-lobed nucleus, indicative of failures in cytokinesis. The nuclear morphology of these HCs appears similar to that reported for the $p21^{Cip1}$-deficient cultured cells exposed to DNA damage (Bunz et al., 1998). These data suggest that $p21^{Cip1}$ is likely involved in both maintenance of the postmitotic state and the establishment of G_2/M checkpoint control in auditory HCs. Interestingly, there was a clear cell-type-specific difference in the degree to which IHCs and OHCs complete an abnormal mitosis in the dko mice. It was mainly IHCs that passed beyond the G_2/M checkpoint, suggesting that mechanisms additional to $p21^{Cip1}$ deficiency may contribute to this checkpoint control in OHCs.

Abnormal proliferation and DNA damage

Consistent with previous data on the apoptotic death of auditory HCs from the $p19^{Ink4d}$ (Chen et al., 2003) and *Rb* mutant (Mantela et al., 2005) mice, the present study shows that abnormal S-phase reentry is a stress factor to these cells. In agreement, it has been shown that genetic inactivation of multiple CKIs *in vivo* leads to neuronal death (Zindy et al., 1999; Cunningham et al., 2002) and overexpression of CKIs *in vitro* promotes neuronal survival (Park et al., 1997). Auditory HCs from the dko mice showed high levels of cyclin E, which, in cell-based studies, alters DNA replication dynamics (Ekholm-Reed et al., 2004). Our data suggest that HCs with abnormal proliferation experience replicative stress that leads to the formation of DSBs in DNA and further to the activation of the DNA damage response and p53-dependent apoptosis. This sequence of events is most clearly indicated by the observations that abnormal DNA replication began before the first signs of activated H2AX, ATM, Chk2, p53, and caspase 3 (Fig. 7). Although HCs from the dko mice showed abrogation of the G_2/M checkpoint and supernumerary IHCs were generated as a result, the fate of these abnormal cells was apoptosis, similar to the cell-cycle-activated HCs that did not proceed beyond the G_2/M transition.

The tumor suppressor p53 is a sensor of cellular stress, being activated in response to various stress signals, such as deregulated proliferation, DNA damage, ischemia, and hypoxia (for review, see Culmsee and Mattson, 2005). We did not find detectable levels of p53 protein in normal HCs. In contrast, p53 was induced in auditory HCs from the dko mice, as manifested by the upregulation of both total p53 protein and its phosphorylated form. Induction of p53 occurred shortly after the onset of S-phase reentry, and this timing correlated with the presence of apoptotic HCs and with HC loss, suggesting that p53 mediates apoptosis in HCs with uncontrolled proliferation. This suggestion is supported by previous *in vitro* data showing that p53 is activated in auditory HCs exposed to cisplatin, a DNA-damaging drug to which inner ear HCs are particularly sensitive, and that a p53 inhibitor (pifithrin-α) protects HCs from cisplatin-induced apoptosis (Zhang et al., 2003).

Based on the phenotype of auditory HCs from the dko mice, we link abnormal cell cycle reentry to activated DNA damage response and apoptosis. Several studies have shown that cell-cycle-related proteins, such as cyclin D and CDKs, are upregulated in postmitotic neurons exposed to various insults and in neurodegenerative diseases (Copani et al., 2001; Yang et al., 2001; Becker and Bonni, 2004; Greene et al., 2004; Herrup et al., 2004). It has also been directly shown that the combination of hypoxia and ischemia can trigger aberrant S-phase reentry of adult neurons *in vivo* (Kuan et al., 2004). In addition, a relationship between aberrant DNA replication and apoptosis induced by DNA damage has been shown in traumatized neurons *in vitro* (Kruman et al., 2004). Correlating these data with the current results, it is possible that at least some types of traumas causing HC death (cisplatin, aminoglycoside antibiotics, and noise) lead to the activation of a DNA damage response pathway either directly or in conjunction with cell-cycle-related proteins and perhaps also to abnormal cell cycle reactivation as part of the apoptotic process. This possibility, however, awaits additional studies. Interestingly, a connection between oxidative stress, mediated through reactive

oxygen species (ROS), and aberrant cell cycle reentry has been suggested in neurodegenerative disorders (for review, see Klein and Ackerman, 2003). Generation of ROS has been associated with trauma-induced HC death (for review, see Henderson et al., 2006), and, thus, as in neurons, one of the actions of oxidative stress in HCs may be to stimulate cell-cycle-related mechanisms, before their death.

Conclusions

Based on the present data, several obstacles are apparent if regrowth of auditory HCs through stimulation of their proliferation is realized, the most critical obstacle being their death-prone phenotype. However, if activation of the cell cycle machinery is a response of HCs to trauma, as frequently appears to be the case in neurons, manipulation of the activity of cell cycle regulators might have therapeutic potential in preventing apoptosis. Therefore, studies on the molecular mechanisms underlying the postmitotic state of HCs are important for the design of future therapies to ameliorate sensorineural hearing loss.

References

Bartkova J, Horejsi Z, Koed K, Krämer A, Tort F, Zieger K, Guldberg P, Sehested M, Nesland JM, Lukas C, Ørntoft T, Lukas J, Bartek J (2005) DNA damage response as a candidate anti-cancer barrier in early human tumorigenesis. Nature 434:864–870.

Becker EB, Bonni A (2004) Cell cycle regulation of neuronal apoptosis in development and disease. Prog Neurobiol 72:1–25.

Bermingham-McDonogh O, Oesterle EC, Stone JS, Hume CR, Huynh HM, Hayashi T (2006) Expression of Prox1 during mouse cochlear development. J Comp Neurol 496:172–186.

Bertwistle D, Zindy F, Sherr CJ, Roussel MF (2004) Monoclonal antibodies to the mouse p19(Arf) tumor suppressor protein. Hybrid Hybridomics 23:293–300.

Brugarolas J, Chandrasekaran C, Gordon JI, Beach D, Jacks T, Hannon GJ (1995) Radiation-induced cell cycle arrest compromised by p21 deficiency. Nature 377:552–557.

Bunz F, Dutriaux A, Lengauer C, Waldman T, Zhou S, Brown JP, Sedivy JM, Kinzler KW, Vogelstein B (1998) Requirement for p53 and p21 to sustain G2 arrest after DNA damage. Science 282:1497–1501.

Chen P, Segil N (1999) $p27^{Kip1}$ links cell proliferation to morphogenesis in the developing organ of Corti. Development 126:1581–1590.

Chen P, Zindy F, Abdala C, Liu F, Li X, Roussel MF, Segil N (2003) Progressive hearing loss in mice lacking the cyclin-dependent kinase inhibitor Ink4d. Nat Cell Biol 5:422–426.

Copani A, Uberti D, Sortino MA, Bruno V, Nicoletti F, Memo M (2001) Activation of cell-cycle-associated proteins in neuronal death: a mandatory or dispensable path? Trends Neurosci 24:25–31.

Culmsee C, Mattson MP (2005) p53 in neuronal apoptosis. Biochem Biophys Res Commun 331:761–777.

Cunningham JJ, Roussel MF (2001) Cyclin-dependent kinase inhibitors in the development of the central nervous system. Cell Growth Differ 12:387–396.

Cunningham JJ, Levine EM, Zindy F, Goloubeva O, Roussel MF, Smeyne RJ (2002) The cyclin-dependent kinase inhibitors $p19^{Ink4d}$ and $p27^{Kip1}$ are coexpressed in select retinal cells and act cooperatively to control cell cycle exit. Mol Cell Neurosci 19:359–374.

Doetzlhofer A, White P, Johnson JE, Segil N, Groves A (2004) In vitro growth and differentiation of mammalian sensory hair cell progenitors: a requirement for EGF and periotic mesenchyme. Dev Biol 272:432–447.

Ekholm-Reed S, Mendez J, Tedesco D, Zetterberg A, Stillman B, Reed SI (2004) Deregulation of cyclin E in human cells interferes with prereplication complex assembly. J Cell Biol 165:789–800.

Greene LA, Biswas SC, Liu DX (2004) Cell cycle molecules and vertebrate neuron death: E2F at the hub. Cell Death Differ 11:49–60.

Hasson T, Gillespie PG, Garcia JA, MacDonald RB, Zhao Y, Yee AG, Mooseker MS, Corey DP (1997) Unconventional myosins in inner-ear sensory epithelia. J Cell Biol 137:1287–1307.

Henderson D, Bielefeld EC, Harris KC, Hu BH (2006) The role of oxidative stress in noise-induced hearing loss. Ear Hear 27:1–19.

Hendzel MJ, Wei Y, Mancini MA, Van Hooser A, Ranalli T, Brinkley BR, Bazett-Jones DP, Allis CD (1997) Mitosis-specific phosphorylation of histone H3 initiates primarily within pericentromeric heterochromatin during G2 and spreads in an ordered fashion coincident with mitotic chromosome condensation. Chromosoma 106:348–360.

Hengst L, Reed SI (1996) Translational control of $p27^{Kip1}$ accumulation during the cell cycle. Science 271:1861–1864.

Herrup K, Neve R, Ackerman SL, Copani A (2004) Divide and die: cell cycle events as triggers of nerve cell death. J Neurosci 24:9232–9239.

Kastan MB, Bartek J (2004) Cell-cycle checkpoints and cancer. Nature 432:316–323.

Klein JA, Ackerman SL (2003) Oxidative stress, cell cycle, and neurodegeneration. J Clin Invest 111:785–793.

Kruman II, Wersto RP, Cardozo-Pelaez F, Smilenov L, Chan SL, Chrest FJ, Emokpae R Jr, Gorospe M, Mattson MP (2004) Cell cycle activation linked to neuronal cell death initiated by DNA damage. Neuron 41:549–561.

Kuan CY, Schloemer AJ, Lu A, Burns KA, Weng W-L, Williams MT, Strauss KI, Vorhees CV, Flavell RA, Davis RJ, Sharp FR, Rakic P (2004) Hypoxia-ischemia induces DNA synthesis without cell proliferation in dying neurons in adult rodent brain. J Neurosci 24:10763–10772.

Livak KJ, Schmittgen TD (2001) Analysis of relative gene expression data using real-time quantitative PCR and the 2(-Delta Delta C(T)) method. Methods 25:402–408.

Lowe SW, Sherr CJ (2003) Tumor suppression by Ink4a-Arf: progress and puzzles. Curr Opin Genet Dev 13:77–83.

Lowenheim H, Furnes DN, Kil J, Zinn C, Gultig K, Fero ML, Frost D, Gummer AW, Roberts JM, Rubel EW, Hackney CM, Zenner HP (1999) Gene disruption of $p27^{Kip1}$ allows cell proliferation in the postnatal and adult organ of Corti. Proc Natl Acad Sci USA 96:4084–4088.

Lu C, Zhu F, Cho Y-Y, Tang F, Zykova T, Ma W, Bode AM, Dong Z (2006) Cell apoptosis: requirement of H2AX in DNA ladder formation, but not for activation of caspase-3. Mol Cell 23:121–132.

Mantela J, Jiang Z, Ylikoski J, Fritzsch B, Zacksenhaus E, Pirvola U (2005) The retinoblastoma gene pathway regulates the postmitotic state of hair cells of the mouse inner ear. Development 132:2377–2388.

Matsui JI, Parker MA, Ryals BM, Cotanche DA (2005) Regeneration and replacement in the vertebrate inner ear. Drug Discov Today 10:1307–1312.

McKeller RN, Fowler JL, Cunningham JJ, Warner N, Smeyne RJ, Zindy F, Skapek SX (2002) The Arf tumor suppressor gene promotes hyaloid vascular regression during mouse eye development. Proc Natl Acad Sci USA 99:3848–3853.

Niculescu III AB, Chen X, Smeets M, Hengst L, Prives C, Reed SI (1998) Effects of p21(Cip1/Waf1) at both the G1/S and the G2/M cell cycle transitions: pRb is a critical determinant in blocking DNA replication and in preventing endoreduplication. Mol Cell Biol 18:629–643.

Nikolic P, Jarlebark LE, Billett TE, Thorne PR (2000) Apoptosis in the developing rat cochlea and its related structures. Brain Res Dev Brain Res 119:75–83.

Park DS, Levine B, Ferrari G, Greene LA (1997) Cyclin dependent kinase inhibitors and dominant negative cyclin dependent kinase 4 and 6 promote survival of NGF-deprived sympathetic neurons. J Neurosci 17:8975–8983.

Pirvola U, Xing-Qun L, Virkkala J, Saarma M, Murakata C, Camoratto AM, Walton KM, Ylikoski J (2000) Rescue of hearing, auditory hair cells and neurons by CEP-1347/KT7515, an inhibitor of c-Jun N-terminal kinase activation. J Neurosci 20:43–50.

Rogakou EP, Pilch DR, Orr AH, Ivanova VS, Bonner WM (1998) DNA double-stranded breaks induce histone H2AX phosphorylation on serine 139. J Biol Chem 273:5858–5868.

Ruben RJ (1967) Development of the inner ear of the mouse: a radioautographic study of terminal mitoses. Acta Otolaryngol (Stockh) [Suppl] 220:1–44.

Sage C, Huang M, Karimi K, Gutierrez G, Vollrath MA, Zhang D-S, García-Añoveros J, Hinds PW, Corwin JT, Corey DP, Chen Z-Y (2005) Proliferation of functional hair cells in vivo in the absence of the retinoblastoma protein. Science 307:1114–1118.

Sage C, Huang M, Vollrath MA, Brown MC, Hinds PW, Corey DP, Vetter DE, Chen ZY (2006) Essential role of retinoblastoma protein in mammalian hair cell development and hearing. Proc Natl Acad Sci USA 103:7345–7350.

Sherr CJ, Roberts JM (1999) CDK inhibitors: positive and negative regulators of G1-phase progression. Genes Dev 13:1501–1512.

Vidal A, Koff A (2000) Cell-cycle inhibitors: three families united by a common cause. Gene 247:1–15.

Vousden KH, Lu X (2002) Live or let die: the cell's response to p53. Nat Rev Cancer 2:594–604.

Weinberg RA (1995) The retinoblastoma protein and cell cycle control. Cell 81:323–330.

Yang Y, Geldmacher DS, Herrup K (2001) DNA replication precedes neuronal cell death in Alzheimer's disease. J Neurosci 21:2662–2668.

Ylikoski J (1974) Guinea-pig hair cell pathology from ototoxic antibiotics. Acta Otolaryngol (Stockh) [Suppl] 326:5–20.

Zhang F, Monkkonen M, Roth S, Laiho M (2002) Proteasomal activity modulates TGF-β signaling in a gene-specific manner. FEBS Lett 527:58–62.

Zhang M, Liu W, Ding D, Salvi R (2003) Pifithrin-alpha suppresses p53 and protects cochlear and vestibular hair cells from cisplatin-induced apoptosis. Neuroscience 120:191–205.

Zhivotovsky B, Kroemer G (2004) Apoptosis and genomic instability. Nat Rev Mol Cell Biol 5:752–762.

Zindy F, Quelle DE, Roussel MF, Sherr CJ (1997) Expression of the p16^{Ink4a} tumor suppressor versus other INK4 family members during mouse development and aging. Oncogene 15:203–211.

Zindy F, Cunningham JJ, Sherr CJ, Jogal S, Smeyne RJ, Roussel MF (1999) Postnatal neuronal proliferation in mice lacking Ink4d and Kip1 inhibitors of cyclin-dependent kinases. Proc Natl Acad Sci USA 96:13462–13467.

Zindy F, van Deursen J, Grosveld G, Sherr CJ, Roussel MF (2000) INK4d-deficient mice are fertile despite testicular atrophy. Mol Cell Biol 20:372–378.

Zindy F, Williams RT, Baudino TA, Rehg JE, Skapek SX, Cleveland JL, Roussel MF, Sherr CJ (2003) Arf tumor suppressor promoter monitors latent oncogenic signals in vivo. Proc Natl Acad Sci USA 100:15930–15935.